Energy-selective (+, +) monolithic monochromator and relative lattice-spacing measurement of Si wafers with synchrotron radiation

Rahman M. Obaidur

Department of Materials Structure Science, The Graduate University for Advanced Studies, Photon Factory, High Energy Accelerator Research Organization – KEK, Oho 1-1, Tsukuba, Ibaraki 305-0801, Japan. E-mail: obaidur@post.kek.jp

X-ray optic systems have been developed at beamline BL-3C2 of the Photon Factory, KEK, for the study of the relative lattice spacings of Si wafers using synchrotron radiation. Since synchrotron radiation has no characteristic (wavelength) spectral lines, unlike an X-ray tube, a new tool has been introduced into the system as a wavelength-selective device – a (+, +) high-resolution channel-cut monolithic monochromator. Using two types of monolithic monochromator, two schemes are proposed and applied to the study of the lattice spacings of Si wafers. The lattice-spacing differences are determined in the sub-p.p.m range; for example, in scheme 1 and scheme 2 we obtain 0.6 p.p.m. and 0.2 p.p.m., respectively. One of the practical advantages of this system is that it can be applied for a fast and precise measurement of the lattice-spacing changes due to the doping and defects in Si, GaAs and other single crystals.

Keywords: monolithic monochromators; quasi-simultaneous diffraction; relative lattice spacing; silicon.

1. Introduction

Lattice-spacing measurements of Si and other single crystals are of importance both for fundamental solid-state physics and applications. For decades Si has routinely been used in the semiconductor industry as well as commonly employed in the beamline optics of synchrotron radiation facilities and other X-ray experiments. Much of the work on lattice-spacing measurement has been reported using well defined wavelengths of laboratory X-ray sources (Cermek, 1960; Cernohorsky, 1960; De Wolf, 1960; Parrish, 1960; Staumanis, 1960; Weyerer, 1960; Wilkens, 1960; Fukumori *et al.*, 1997). In contrast, relatively few works have been reported using state-of-the-art synchrotron radiation (SR) X-ray sources (Beaumont & Hart, 1974; Usuda, 1994; Rahman *et al.*, 1998; Rahman, Sugiyama *et al.*, 1999).

Unlike X-ray tube data, for which tables of wavelengths of the characteristic spectral lines are available, there are no lines in the SR spectrum. Therefore it is necessary to make schemes and data available for precise determinations of lattice spacing which utilize SR sources. Thus one of our main motivations is to develop a high-precision relative lattice-spacing-measurement system using SR for SR users. In addition, the methods can be applied to other applications, *e.g.* for the measurement of relative lattice-spacing changes due to the B-doping in Si, B-doping in VBG LEC GaAs, and As- and In-doping in GaAs crystals, to mention a few. One of the main advantages of these systems is that in most applications one does not require a highly accurate absolute value of the wavelength, only a relative high-precision value.

To this end, we have constructed two X-ray optics systems for relative high-precision lattice-spacing measurement of single crystals using synchrotron radiation at BL-3C2 of the Photon Factory, KEK. In our new optics, an energy-selective (+, +) channel-cut monolithic monochromator together with a higher-angle-resolution goniometer with a precision of 0.36 arcsec have been introduced. We have designed and fabricated several kinds of monolithic monochromator (MM) that give a fixed exit beam position and provide a convenient setting of the whole X-ray optics. With the current set-up it is simple to make another d-spacing measurement, if need be, by simply replacing the monochromator with another. In addition to the measurements of Si crystals, measurements for other materials, such as GaAs crystals, can easily be performed. The monolithic double-crystal monochromator is obtained from a single perfect crystal as a means of obtaining an X-ray beam of well defined wavelength. A monolithic monochromator is, in effect, a single perfect crystal where two sets of Bragg planes play the role of two seperate crystals. As the interplanar angle between the concerned diffraction plane is fixed in the MM, the wavelength emerging from this device is highly stable and is extremely stable against temperature variations. The two types of MM allow us to propose two schemes for the lattice-spacing measurement. Approximately, the precision achieved in $\Delta d/d$ in these systems is in the range 10^{-7}–10^{-8}. The method has been applied (Rahman & Ando, 2001; Okada *et al.*, 1998; Rahman, Okada *et al.*, 1999) for the B-doped Si and B-doped VBG LEC GaAs single crystals. From these measurements we can see that the lattice-spacing changes can be modelled by Vegard's law. The method can be applied to study the lattice-spacing changes due to the doping, defects in the single crystal and further to study the photon–phonon energy transfer in inelastic scattering experiments. The two proposed systems are ready for use at SR facilities.

The layout of this paper is as follows. In the following section we discuss the MM. This is followed by experimental details of our proposed schemes and the measurements made. We then briefly mention computer control employed in our set-up and applications. Applications will be undertaken in more detail in a later note. §6 is devoted to results and discussion. Finally, conclusions are stated.

2. Monolithic monochromator

The starting point of the monolithic monochromator design is Bragg's law. In order to obtain suitable wavelength for experiments from the MM, we consider the following three equations,

$$\lambda_1 = \lambda = 2d_1 \sin\theta_1\left(1 - \delta/\sin^2\theta_1\right),$$
$$\lambda_2 = \lambda = 2d_2 \sin\theta_2\left(1 - \delta/\sin^2\theta_2\right),$$
$$\theta_1 + \theta_2 + \beta_0 = \pi,$$

where δ represents the real part of the refraction index, β_0 is the interplanar angle between the two planes, and θ_1 and θ_2 are the Bragg angles for two diffraction planes d_1 and d_2, respectively.

If $\delta = 0$, the equations simplify and yield, after simple algebra,

$$\lambda = \frac{2d_1 \sin\beta_0}{\left\{\left[\left(h_2^2 + k_2^2 + l_2^2/h_1^2 + k_1^2 + l_1^2\right)^{1/2} - \cos\beta_0\right]^2 + \sin^2\beta_0\right\}^{1/2}}. \quad (1)$$

If $d_1 = d_2 = d$, equation (1) further reduces to

$$\lambda = \frac{2d \sin\beta_0}{\left[(1 - \cos\beta_0)^2 + \sin^2\beta_0\right]^{1/2}}. \quad (2)$$

Using (1) and (2), a simulation code *MMCD* [monolithic monochromator crystal design] has been realised which can generate different wavelengths using (h_1, k_1, l_1) and (h_2, k_2, l_2) combinations. Our code relies on the Deslattes & Henins (1973) lattice spacing of silicon wafer of $d_{220} = 1.9201715 \pm 0.0000006$ Å at 278 K. Two types

Table 1
Type 1 and type 2 simulated wavelength from *MMCD* computer code.

Type 1: different indexes. Type 2: same indexes.

$h_1k_1l_1$	$h_2k_2l_2$	HKL	β_0	θ_1	θ_2	λ	δ
Type 1							
1 5 5	$\bar{5}$ 3 1	$\bar{4}$ 8 6	69.2044	63.1437	47.6519	1.356950	0.57719×10^{-5}
3 5 5	$\bar{3}$ 3 1	0 8 6	70.8196	75.8031	33.3772	1.370938	0.58915×10^{-5}
3 3 5	$\bar{3}$ 5 1	0 8 6	73.5280	57.1730	49.2990	1.391940	0.60734×10^{-5}
1 1 3	$\bar{5}$ $\bar{3}$ 5	$\bar{4}$ $\bar{2}$ 8	74.0515	25.2230	80.7255	1.395642	0.61057×10^{-5}
1 1 3	$\bar{3}$ $\bar{5}$ 5	$\bar{2}$ $\bar{4}$ 8	74.0515	25.2230	80.7255	1.395642	0.61057×10^{-5}
1 5 5	5 1 5	6 6 10	46.6641	66.6680	66.6680	1.396621	0.61143×10^{-5}
1 1 3	$\bar{5}$ 3 1	$\bar{4}$ 4 2	104.7631	25.3769	49.8599	1.403594	0.61755×10^{-5}
3 5 5	1 5 $\bar{1}$	4 10 4	54.8119	83.0088	42.1792	1.403614	0.61757×10^{-5}
1 1 5	1 1 7	2 2 12	42.4407	68.3502	69.2091	1.410846	0.62686×10^{-5}
Type 2							
1 3 5	3 $\bar{5}$ $\bar{1}$	4 $\bar{2}$ 4	119.0593	30.4704	30.4704	0.931039	0.27172×10^{-5}
3 5 5	$\bar{5}$ $\bar{3}$ 5	$\bar{2}$ 2 10	94.8614	42.5693	42.5693	0.956631	0.28686×10^{-5}
1 3 5	5 $\bar{1}$ $\bar{3}$	6 2 2	111.8037	34.0981	34.0981	1.029302	0.33210×10^{-5}
3 3 5	$\bar{3}$ 5 $\bar{3}$	0 8 2	102.0815	38.9593	38.9593	1.041527	0.34004×10^{-5}
1 5 5	$\bar{1}$ $\bar{5}$ 5	0 0 10	91.1235	44.4382	44.4382	1.064914	0.35548×10^{-5}
1 3 5	$\bar{5}$ $\bar{3}$ 1	$\bar{4}$ 0 6	104.9006	37.5497	37.5497	1.118970	0.39249×10^{-5}
1 5 5	$\bar{5}$ 5 $\bar{1}$	$\bar{4}$ 10 4	72.8954	53.5523	53.5523	1.223493	0.46924×10^{-5}
3 3 5	$\bar{3}$ $\bar{3}$ 5	0 0 10	80.6311	49.6854	49.6854	1.263037	0.50006×10^{-5}
1 3 5	$\bar{5}$ 3 $\bar{1}$	$\bar{4}$ 6 4	91.6373	44.1814	44.1814	1.279591	0.51325×10^{-5}
1 5 5	5 5 1	6 10 6	46.6641	66.6680	66.6680	1.396621	0.61143×10^{-5}
1 3 5	$\bar{3}$ 5 $\bar{1}$	$\bar{2}$ 8 4	78.4630	50.7685	50.7685	1.223493	0.46924×10^{-5}
3 3 5	$\bar{3}$ $\bar{3}$ 5	0 0 10	80.6311	49.6854	49.6854	1.422186	0.63402×10^{-5}
1 1 5	$\bar{1}$ 5 $\bar{1}$	0 6 4	92.1226	43.9387	43.9387	1.450516	0.65953×10^{-5}
1 3 5	$\bar{1}$ $\bar{3}$ 5	0 0 10	64.6231	57.6885	57.6885	1.551732	0.75479×10^{-5}
1 3 5	5 3 1	6 6 6	57.1216	61.4392	61.4392	1.612607	0.81517×10^{-5}

of MM have been designed and fabricated on the basis of (1) and (2). These are notated by type 1 and type 2. Type 1 is used in the experimental set-up, refered to as scheme 1, and, similarly, type 2 is utilized in the set-up called scheme 2.

Figs. 1 and 2 show the MMs that have been made for the wavelengths defined by equations (1) and (2), respectively. Some of the simulated wavelengths from the *MMCD* code are given in Table 1 for both types of MM, with refraction correction δ, given by $\delta = 4.48 \times 10^{-6} n_0 \lambda^2$. Here, n_0 is the number density, *e.g.* $n_0 = 699\ \mathrm{nm}^{-3}$ for Si, and λ is the wavelength of the X-rays.

For illustration, we reproduce the following two examples:

Type 1: MM diffraction planes $d_1 \neq d_2$, wavelength λ = 0.1410846 nm. This monolithic monochromator has been made using the reflection indexes (1, 1, 7), (1, 5, 1), $(\bar{1}, \bar{1}, \bar{7})$ and $(\bar{1}, \bar{5}, \bar{1})$, which is an implementation of equation (1). The motivation behind the fabrication of this monochromator is to study the *d*-spacing of an Si single crystal as well as a GaAs(800) single crystal. As the high Bragg angle provides high precision, we found that the above indexes from the *MMCD* code provide 86.5° for the GaAs(800) sample. Table 2 shows some of the monochromator wavelengths that we have made, together with their design parameters.

Type 2: MM diffraction plane $d_1 = d_2$, wavelength λ = 0.1612607 nm. This monochromator has been designed having the same Bragg angle for (h_1, k_1, l_1) and (h_2, k_2, l_2). The indexes being used are (5, 1, 3) and (1, 5, 3), which are an implementation of equation (2). The reason for choosing this wavelength and these indexes originates from the advantage of precision lattice-spacing measurement for Si. The conventional Bond method (Bond, 1960) usually provides a high-precision value but a rotation of the sample is required for the Bond method. If we choose indexes (5, 1, 3) and (1, 5, 3) of the samples and a wavelength of 0.162160 nm, we can achieve quasi-simultaneous diffraction instead of rotation of the sample and thus the effect of temperature will be smaller, measurement time will be shortened and more precise data can be obtained than the conventional Bond method at room temperature.

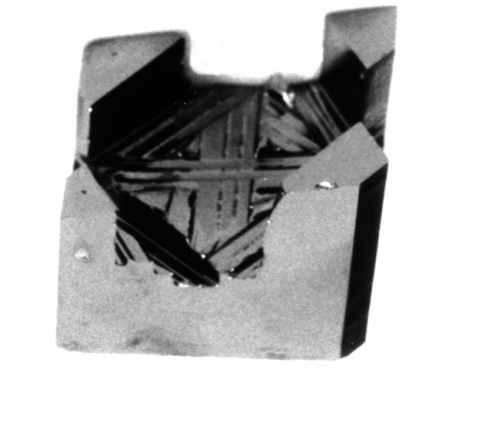

Figure 1
Type 1 monolithic monochromator designed for a wavelength of 0.1410 nm with index (1, 5, 1), (1, 1, 7), $(\bar{1}, \bar{5}, \bar{1})$, $(\bar{1}, \bar{1}, \bar{7})$.

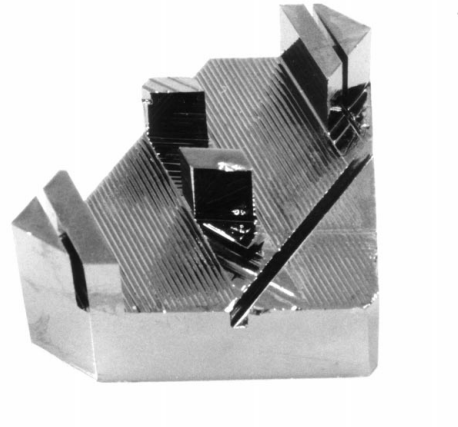

Figure 2
Type 2 monolithic monochromator for a wavelength of 0.1612 nm with index $(\bar{5}, 1, 3)$, (1, 5, 3), $(\bar{5}, \bar{1}, \bar{3})$, $(\bar{1}, \bar{5}, \bar{3})$.

2.1. Precision provided by the MM

The full width at half-maximum (FWHM) of the reflecting range of an MM is determined by the dynamical theory of diffraction and is given by

$$\Delta\theta = 2C\chi_g\left(\gamma_g/\gamma_0\right)^{1/2}/\sin 2\theta_{\mathrm{B}},$$
$$\chi_g = -\gamma_e\lambda^2 F_h/\pi V_c,$$

where γ_e is the classical electron radius, F_h is the atomic structure factor, V_c is the volume of the unit cell, λ is the wavelength and C is

Table 2
Monochromator and some of their design parameters.

Diffraction planes	Bragg angles θ_1, θ_2 (°)	Wavelength (nm)	$L \times B \times H$ (mm)	Beam gap (mm)	$\Delta\lambda/\lambda$ ($\times 10^{-6}$)	$\Delta\theta$ ($\times 10^{-6}$)
(5 9 11), $(7\ \bar{7}\ \bar{7})$	74.30, 50.77	0.0694067	45 × 40 × 40	7	0.5	1.6
$(3\ 3\ \bar{3})$, $(\bar{3}\ \bar{5}\ \bar{3})$	47.53, 68.58	0.1542067	55 × 52 × 50	29	2.8	9.2
(1 5 1), (1 1 7)	42.44, 68.06	0.1410846	35 × 42 × 35	15	2.5	8.7
(5 1 3), (1 5 3)	61.43, 61.43	0.1612607	60 × 55 × 37	35	4.3	0.1
(1 5 5), $(\bar{5}\ 3\ 1)$	62.78, 47.65	0.1352569	40 × 30 × 35	0	2.3	6.2

the polarization factor ($C = 1$ for σ polarization and $C = \cos 2\theta_B$ for π polarization). We note that $(\gamma_g/\gamma_0) = 1$ for a symmetric reflection. As an example of an MM designed for a wavelength of 0.1410846 nm, the calculated angular divergence and wavelength spreads are given by $\Delta\lambda/\lambda = 2.5 \times 10^{-6}$ and $\Delta\theta = 8 \times 10^{-6}$ rad. All monochromators were well characterized in terms of their throughput, wavelength and angular resolution. The experiment was carried out at beamline BL-3C2 (Rahman *et al.*, 1998; Rahman, Sugiyama *et al.*, 1999) which is located on the 2.5 GeV ring of the Photon Factory.

2.2. Synchrotron X-rays

As is well known, some of the advantages of SR compared with conventional X-ray generator tubes are higher intensity, wavelength selectivity and well colliminated beam. Many devices have been, and are being, developed to further increase the intensity, such as wigglers, undulators and X-ray FELs. We used the standard bending-magnet radiation which gave at least an order of magnitude higher intensity and better resolution than the X-ray tube. The much higher statistics and lower background obtained with SR are important factors in precision measurements. The question arises as how to extract exact values for wavelength. For X-ray tubes there is a guiding principle, since tables of wavelengths of the characteristic spectral lines are readily available. In contrast, there are no lines in the SR spectrum. Only the absorption edges of elements in the specimen or of thin foils placed in the beam can be measured. The accuracy of such measurements is not as high as desired because of the uncertainty as to what feature of the edge should be used as a measure of wavelength.

The wavelength problem could be avoided by using the ratio of the lattice parameters of the specimen to an accurately known standard. The limitation is, of course, the accuracy of the standard. The extraction of a standard for exact wavelength determination will be discussed elsewhere. For the purpose of the current work we limit our discussion to the following: for determination or calibration of wavelength we use FZ Si(444) as a reference, which is oxygen-free, and the lattice-parameter change has been determined to be about 2×10^{-8}. The callibration was performed before and after a series of experiments and no change was detected, showing the stability of our measurement technique.

3. Experimental

3.1. Measurement of lattice spacing of Si-wafers single crystals

3.1.1. Scheme 1 with type 1 MM diffraction planes $d_1 \neq d_2$. This scheme is a modification of the Bond method (Bond, 1960) with MM X-ray optics. We have carried out an experiment for the precision lattice-spacing measurement of Si using SR from bending magnets. Fig. 3(*a*) shows a schematic diagram of the experimental set-up. The novelty of the scheme is that we can replace the MM and sample in each experiment. Several experiments have been carried out using the above scheme. We describe here the case where an MM of wavelength 0.1410846 nm and sample Si(444) FZ are used. The experiments for the other cases, *i.e.* with different MM wavelengths, follow almost the same procedure and only the results will be reported. As can be seen in Fig. 3(*a*), a channel-cut MM has been introduced using the geometry of successive lattice planes (1, 5, 1) and (1, 1, 7) and a wavelength of 0.1410846 nm was obtained. In the experimental scheme of Fig. 3(*a*), the SR X-ray beam from the channel-cut monochromator is diffracted from an Si(444) sample crystal at a crystal angle $W1$ (diffraction maxima) into detector PIN #1 on the left-hand side. The same Bragg reflection is also observed at a crystal position $W2$ (diffraction maxima) with detector PIN #2 on the right-hand side. The change in crystal angle $(180 - 2\theta_B)$ is independent of the goniometric errors and now one can obtain the Bragg angle using the Bond formalism (Bond, 1960). Necessary tilt adjustments both for the channel-cut crystal and sample crystal have been made. The centre of the goniometer, holding the Si(444) sample fixed, was adjusted by taking X-ray photographs so that the centre of the beam from the monochromator would hit the centre of the rotation axis of the goniometer. We also used the laser (He–Ne) beam to adjust the beam height and position. A rotary encoder with a precision of 0.36 arcsec was used to record the $W1$ and $W2$ values. An automated computer system has been installed to run the experiment and to store the data (see §4). Table 3 shows the $W1$ and $W2$ values for Si(444). The average value for nine measurements of an Si wafer is reported as $d_{obs} = 0.078390564 \pm 3 \times 10^{-8}$ nm at 298 K. The average $\Delta d/d$ was obtained as 6.2×10^{-7}, calculated from d(cal) and d_{obs}. The results of $\Delta d/d$ for Si FZ and GaAs(800) samples are reported in Table 4.

3.1.2. Scheme 2 with type 2 MM diffraction planes $d_1 = d_2$. In this scheme, two equivalent lattice planes have been chosen for the sample for a particular wavelength, thus providing two almost simultaneous diffractions with a few arcsec rotation of the sample. The scheme of the system is shown in Fig. 4(*a*). In this scheme, a four-reflection-type MM having diffraction planes $d_1 = d_2$ has been

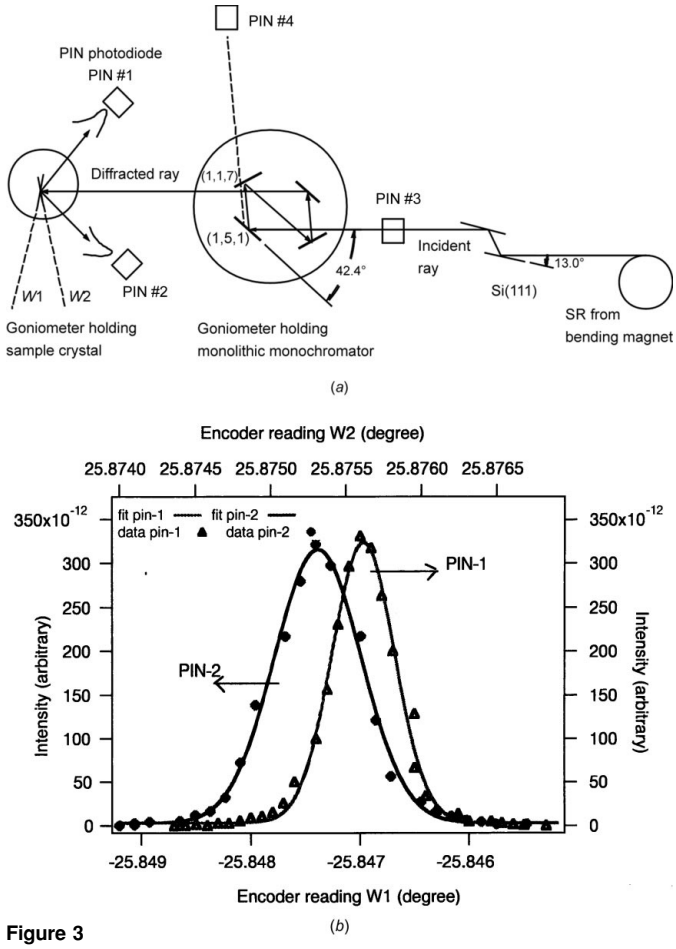

Figure 3
(*a*) Scheme 1: SR from the bending magnet incident on the Si(111) double-crystal monochromator and, after four reflections from the MM (0.1410 nm), impinges on sample Si(444). Two diffractions are recorded at the PIN #1 and PIN #2 detectors. $W1$ and $W2$ values are recorded using a Heiden heigh encoder. (*b*) Pair of diffraction curves observed in scheme 1 from the Si +(444) and −(444) planes.

Table 3
Relative lattice spacing for Si(444) wafer sample with MM of 0.1410 nm wavelength.

Measurement number	Left peak, $W1$ (°)	Right peak, $W2$ (°)	Difference, $W1 - W2$ (°)	d-value (corrected) (nm)	Average $\Delta d/d$ ($\times 10^{-7}$)
1	215.3518	163.6417	51.7101	0.078390514	
2	215.3526	163.6419	51.7107	0.078390713	
3	215.3516	163.6409	51.7107	0.078390713	
4	215.3525	163.6412	51.7113	0.078390912	
5	215.3525	163.6418	51.7107	0.078390713	6.2
6	215.3514	163.6428	51.7186	0.078390017	
7	215.3514	163.6410	51.7104	0.078390613	
8	215.3514	163.6423	51.7191	0.078390173	
9	215.3518	163.6411	51.7107	0.078390713	

introduced as a fixed-wavelength device. A monolithic monochromator that uses (5, 1, 3), (1, 5, 3), $(\bar{5}, \bar{1}, \bar{3})$, $(\bar{1}, \bar{5}, \bar{3})$ reflections has been made from a channel-cut Si crystal grown along the [111] direction and provides the wavelength $\lambda = 0.16126$ nm. This wavelength satisfies the simultaneous Bragg condition for the indexes (5, 1, 3), $(\bar{5}, \bar{1}, \bar{3})$, (1, 5, 3) and $(\bar{1}, \bar{5}, \bar{3})$. The Bragg angles for both

Table 4
Relative lattice-spacing values measured using scheme 1 for Si and GaAs samples.

Sample number	Sample type	Sample index	MM wavelength (mm)	Average $\Delta d/d$ ($\times 10^{-7}$)
Si	FZ	(444)	0.1542	6.1
Si	CZ	(800)	0.1356	6.3
GaAs	CZ	(800)	0.1356	8.0

indexes is 61.4392° and the interplanar angle is 57.1216°. In this setup, MM crystal faces are arranged in a (+, +, −, −) dispersive setting. The four crystal faces of the monochromator are the inner faces of channel-cut crystals of Si. This method has been applied for the measurement of the d-spacing of FZ Si-wafer, the sample indexes chosen being (5, 1, 3) and (1, 5, 3), which provide the same Bragg angle. The sample was selected FZ Si orientation flat of 110, normal direction of 111. When an X-ray beam of wavelength 0.16126 nm is projected onto the sample along the [111] direction, Bragg conditions for (5, 1, 3) and (1, 5, 3) are satisfied and thus we observed the two diffractions simultaneously. The measured Bragg angle is determined

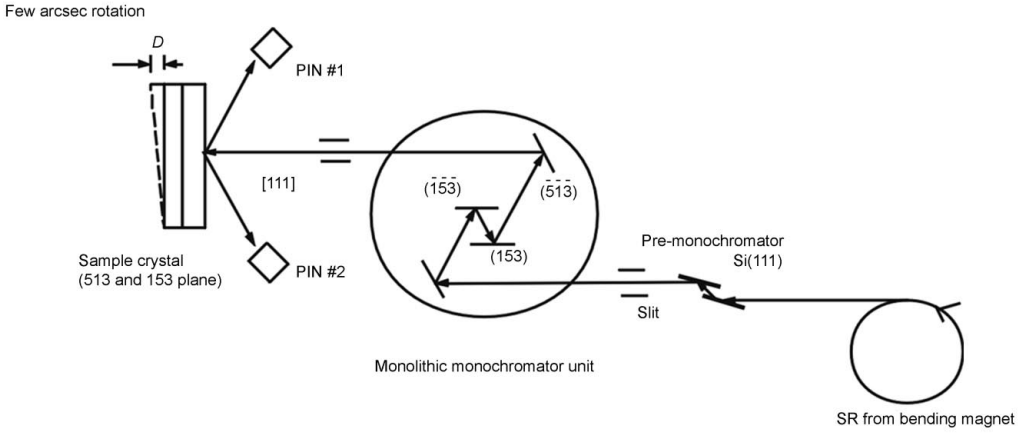

(*a*)

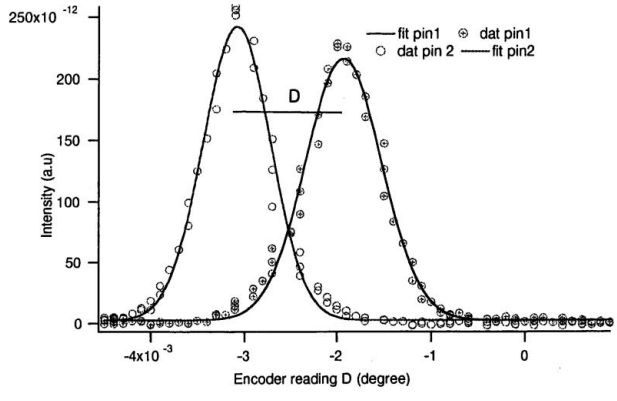

(*b*)

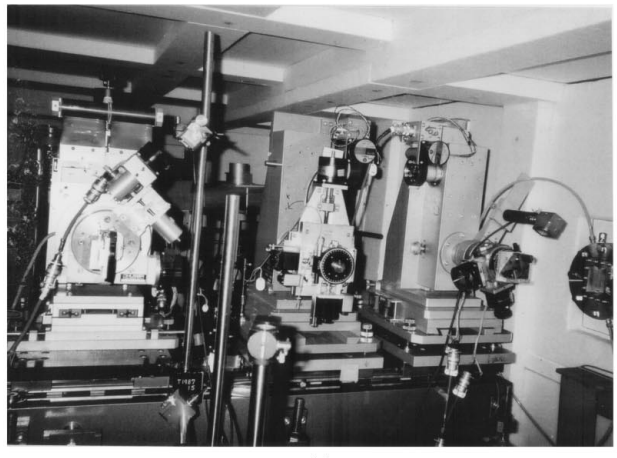

(*c*)

Figure 4
Scheme 2: SR from the bending magnet incident on the Si(111) double-crystal monochromator and, after four reflections from the MM (0.1612 nm), impinges on sample Si(153). Two diffractions are recorded at the PIN #1 and PIN #2 detectors. The differences between the two peaks' D values are recorded using a Heiden heigh encoder. (*b*) Pair of diffraction curves observed in scheme 2 from the Si (513) and (153) planes. (*c*) Photographic view of scheme 2. A goniometer near to the beam port is used for the MM with two tilt stages; a third goniometer is used for the Si(153) sample wafer; two PIN detectors are set to record the two quasi-simultaneous diffractions.

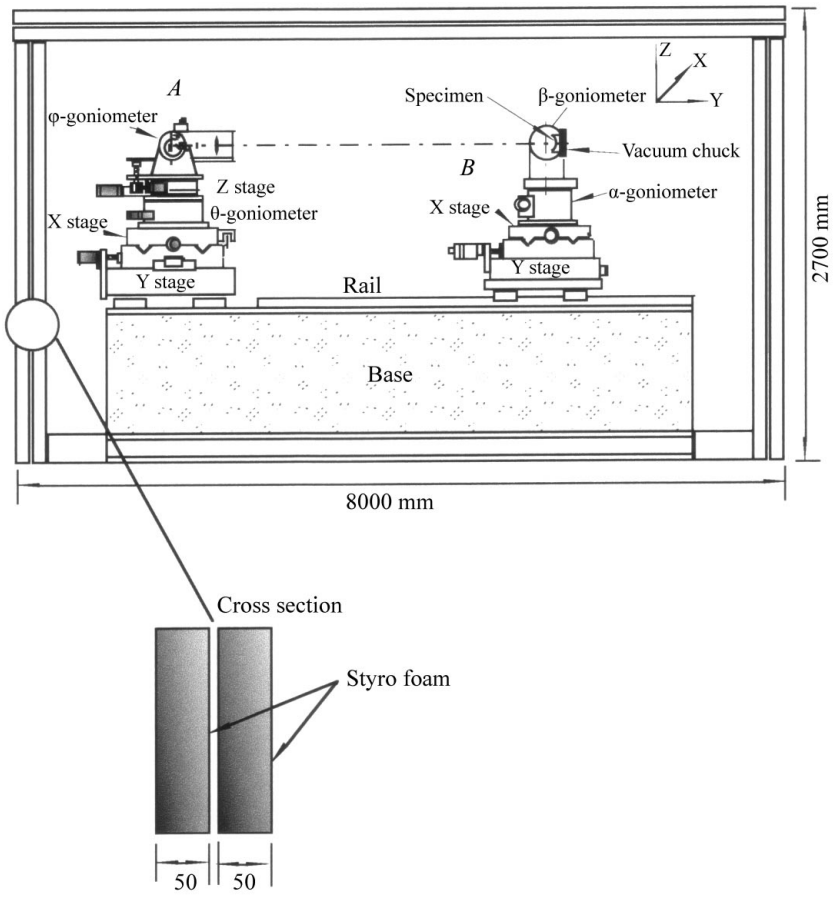

Figure 5
Temperature passive controlled cleaned hutch covered with styro foam; goniometer *A* can be used for the MM and goniometer *B* for the sample.

by the geometry of the experiment and is given by $\theta_B = 90^\circ - \beta_0/2 - D$, where D is the peak difference between the two rocking curves (5, 1, 3) and (1, 5, 3) (see Fig. 4*b*). For two such measurements, $\Delta\theta \propto \Delta D$, thus ΔD is a direct measure of the change in relative lattice-spacing from the differential of Bragg's law, $\Delta d/d = -\cot\theta\Delta\theta$.

In this experiment, the polarization of the SR is chosen as horizontal and the diffraction plane is chosen vertical and there is no multiple beam effect (Colella, 1974) in the set-up adopted. Two goniometers have been used for the monochromator and sample crystal. The axis of the goniometer has been adjusted perpendicular to the X-ray beam by laser. The goniometer containing the MM has two tilt axes, one parallel to the first diffraction plane and the other perpendicular to the plane. Fig. 4(*c*) shows a photographic view of the set-up. In our system, several thermistor probes were used for temperature measurement at both the MM and at the sample. The entire experimental hutch was covered by styro foam, and the temperature fluctuation was controlled to within ± 0.01 K. Fig. 5 shows the passive temperature-controlled clean hutch: *A* is used for the MM and *B* for the specimen. A refraction correction has been taken into account, *i.e.* $d = d_0(1 - 4\,d_0^2\,\delta/\lambda^2)$, where $\delta = 4.48 \times 10^{-6} n_0 \lambda^2$, where $n_0 = 699\ \mathrm{nm}^{-3}$ for Si. The measured d_{153} value in our experiment was, on average, 0.091801632 $\pm$ 2 $\times$ 10^{-8} nm.

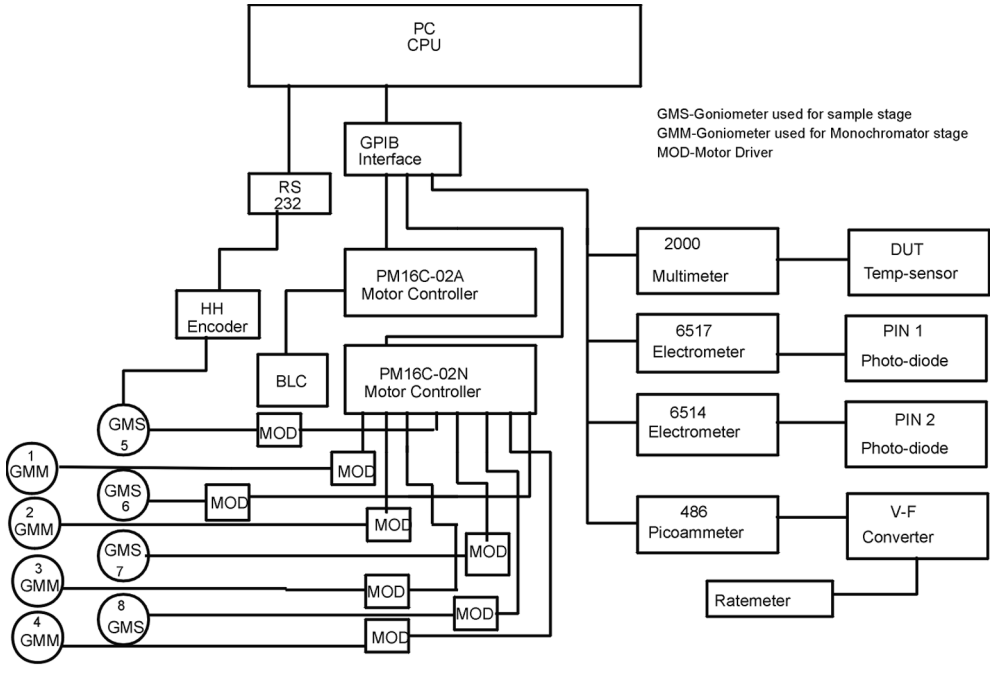

Figure 6
Computer-controlled block diagram for the relative lattice-spacing measurement system.

4. Computer control

An automated computer system has been installed to run the experiment and to store the data. During the measurement, the computer automatically drove pulse motors for the goniometers, counted X-ray intensities, and saved data in the memory. After all the measurements are finished, the peak positions of the rocking curve were determined through a curve-fitting procedure, assuming a distribution $y = I_p/[1 + a(X - \theta_p)^2]$, where I_p is the peak intensity, θ_p is the peak position and $2/a^{1/2}$ is the FWHM. The computer processed a least-squares fitting to obtain the peak position, calculated the Bragg angle and also determined the lattice spacings with corrections. A block diagram for the control system is shown in Fig. 6. In this system, eight motor control systems have been used to run the MM and sample goniometer stage, and several GPIB interfaces have been used to run the beamline optics and experimental optics. A multimeter and pico-ammeter are used to record the intensity from the PIN photodiode. Two 16-channel pulse motor controller systems are connected to a motor-driving system which is further connected to several goniometer stages holding the sample (GMS) and monochromator stages (GMM). Therefore, sample scanning and the MM setting are controlled from outside the hutch. A temperature-controlled system has been developed to monitor the temperature using a 7015 multiplexer coupled with a 2000 multimeter. Fig. 7 shows one of the temperature records before and after the lattice-spacing measurement as an example. Ten temperature probes have been installed to monitor the temperature at the MM, at the sample and at various positions of the hutch (Rahman, 2001). The entire hutch was covered by styro foam and is shown in Fig. 5. Furthermore, vibration spectra have been recorded using a Fourier spectrometer. Fig. 8 shows the spectrum when the accelerometer sensor is placed on the sample goniometer stage, and Fig. 9 shows the spectrum when the sensor is put on the sample holder during the goniometer movement by the motor. We observed from both spectra that there are no significant changes; the peaks are due to the a.c. line signal in the experimental hutch, thus the lattice-spacing values are error-free owing to the pressure which may cause 1/3 p.p.m. per bar.

5. Applications

Applications of the methods for lattice-spacing changes to B-doped Si and VBG LEC GaAs crystals have been reported elsewhere (Rahman & Ando, 2001; Okada *et al.*, 1998; Rahman *et al.*, 1999). The results demonstrate that the lattice-spacing changes can be modelled by $\Delta a = a_0 \times (r_i - r_s)/r_s \times (N_i/N_s)$, where r_i and r_s are the radii of impurities and silicon atoms, respectively, and N_i and N_s are the concentration of impurities and silicon. This is in good agreement with Vegard's law. Furthermore, several new states have been observed in addition to the Vegard's states in the case of B-doped VBG LEC GaAs crystals. The presented methods are useful in the study of the lattice-spacing changes induced by the defects, and doping in single crystals. Moreover, it is possible to study phenomena such as photon–phonon energy transfer in inelastic scattering due to the high-resolution X-ray optics used in the current set-up. A more detailed discussion of the applications of the methods mentioned will be discussed elswhere.

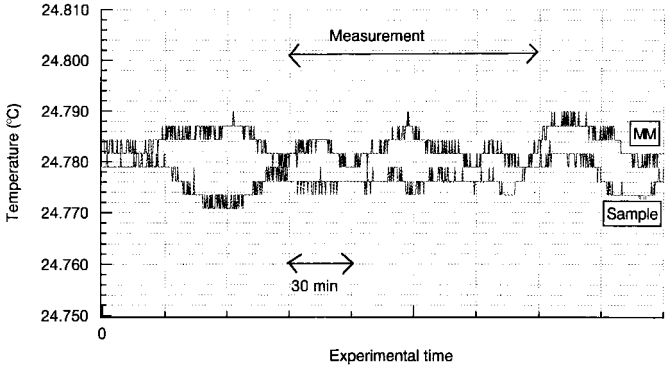

Figure 7
Temperature variation in the MM and sample during the experiment. The fluctuation is within 0.01 K.

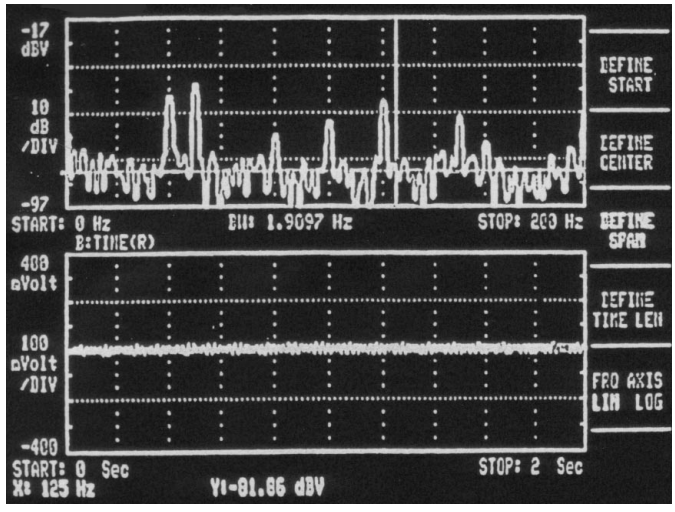

Figure 8
Vibration spectrum in db when the accelerometer sensor is placed on the sample stage of the goniometer. The peak signals are due to the line signal in the hutch.

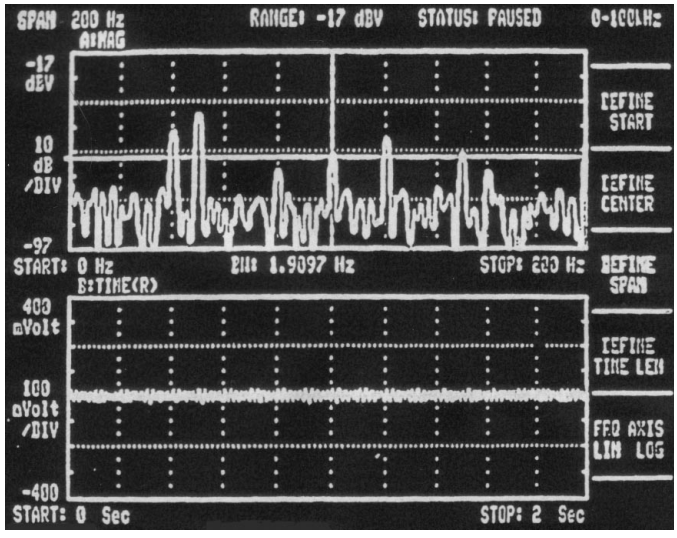

Figure 9
Vibration spectrum in db when the accelerometer sensor is placed on the sample holder. The peak signals are due to the line signal in the hutch.

6. Results and discussion

As mentioned above, two relative lattice-spacing measurement methods using two types (*i.e.* scheme 1 and scheme 2 based on the diffraction plane conditions $d_1 \neq d_2$ and $d_1 = d_2$, respectively) of (+,+) energy-selective MM with SR have been developed. Results of the two schemes are summarized in this section.

In scheme 1 we applied our method to several MMs, as shown in Tables 3 and 4. The novelty of the method is that in each case the MM and sample can be changed. For the Si sample grown by FZ and for the plane (444) an MM wavelength of 0.1410 nm is utilized. Fig. 3(*b*) shows the pair of diffraction curves for this case. The results for this case are summarized in Table 3. Nine measurements were taken at different positions of the Si wafer and the corrected d values are listed. The average value of $\Delta d/d$ is 6.2×10^{-7}, as mentioned earlier. Table 4 shows the results of our lattice-spacing measurement for Si grown by CZ and FZ methods where the planes (800) and (444) are considered in addition to GaAs grown by the CZ method for the plane (800). We can see that the average value of $\Delta d/d$ is higher for GaAs compared with that of Si. Temperature and refraction corrections have been taken into account. For scheme 1, several temperature probes were installed at the sample and the MM. The true value of d is given by $d_{\rm obs} + \Delta d_r + \Delta d_t$, where Δd_r and Δd_t are the refraction and temperature corrections, respectively. The refraction correction is calculated for a 0.1410 nm wavelength as 0.0000019 Å and the temperature correction was 0.000006 Å to the d value. The calculated d value has been taken at 298 K from Deslattes & Henins (1973); the measured d_{444} value obtained on the average of nine measurement points is $0.078390564 \pm 2 \times 10^{-8}$ nm. In scheme 2, two equivalent planes and a few arcsec rotation (D) of the samples provide two quasi-simultaneous Bragg diffractions. This method is fast. Several scans were performed for Si wafers prepared using the FZ method and two diffraction profiles were recorded from the (5, 1, 3) and (1, 5, 3) planes. Fig. 4(*b*) shows this scheme with a pair of diffraction curves from the (5, 1, 3) and (1, 5, 3) planes. Fig. 10 shows the results of 70 measurements taken at different positions of a Si(153) FZ-prepared wafer. From this graph we can see that the approximate average value of $\Delta d/d$ is 1.1×10^{-7}. The temperature variation has been carefully monitored. For scheme 2, several temperature probes were installed at the sample and the MM. The true value of d is given by $d_{\rm obs} + \Delta d_r + \Delta d_t$, where Δd_r and Δd_t are the refraction and temperature corrections, respectively. The refraction correction is calculated for wavelength 0.16126 nm as 0.00000749 Å and the temperature correction was 0.00000291 Å to the d value. The measured d_{153} value obtained on the average of 70 measurement points is $0.091801632 \pm 2 \times 10^{-8}$ nm. As Fig. 10 shows for 70 measurements, the $\Delta d/d$ value obtained from ΔD is within the 0.2 p.p.m. level. The standard deviation calculated from 100 measurements of the differential peak difference D at one point was 2×10^{-8}.

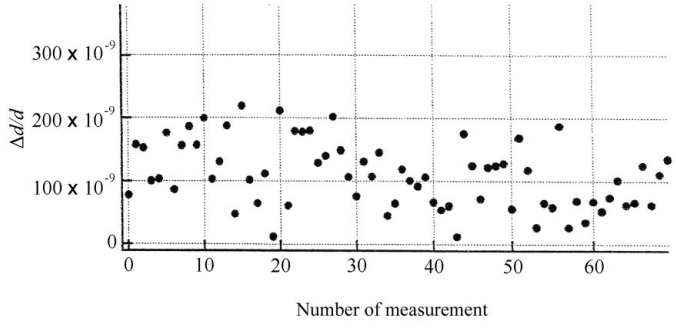

Figure 10
The relative lattice-spacing changes for 70 measurement points of an Si(153) wafer. The precision is within 0.2 p.p.m.

7. Conclusions

In conclusion, keeping in mind the unique features of SR such as high intensity, tunability and high-resolution d-spacing, two measurement systems have been developed at the Photon Factory, KEK, and successfully operated and tested. The system can be used in a routine d-spacing measurement of Si and other single crystals with a precision of 10^{-7} to 10^{-8}. Both systems are inexpensive and each measurement takes only a few tens of seconds. The accuracy of both methods is determined by the tilt adjustment of the MM, geometric misalignment, peak determination of the profiles and the fluctuation of the wavelength and the stability of SR. In scheme 2 we have demonstrated a method for Si lattice-spacing measurement which only requires a few arcsec rotation of the sample, thus bypassing the larger rotation (of the order of a few degrees) of the sample required in the conventional Bond method. As the two pairs of diffractions occur almost simultaneously, each measurement therefore takes only a few seconds. Thus, our new system is speedy, accurate and highly stable. The method is suitable for improving the accuracy of measuring the lattice parameter, which in turn is needed for the determination of the exact wavelength used. The applications of the methods for lattice-spacing changes to B-doped Si and VBG LEC GaAs crystals have been reported elsewhere (Rahman & Ando, 2001; Okada *et al.*, 1998; Rahman *et al.*, 1999). The results demonstrate that the lattice-spacing changes can be modelled by $\Delta a = a_0 \times (r_i - r_s)/r_s \times (N_i/N_s)$, where r_i and r_s can be regarded as the radius of impurities and silicon atoms, and N_i and N_s are the concentration of impurities and silicon. This is in agreement with Vegard's law. Furthermore, several new states have been observed in addition to the Vegard's states in the case of the B-doped VBG LEC GaAs crystal. The presented methods open up a new direction in solid-state research, in particular in the study of changes in the lattice spacing due to the defects, and doping in single crystals. This is made possible owing to the high-resolution X-ray optics used in the set-up described here. Furthermore, it is hoped that the monolithic monochromator and the systems developed will result in a more widespread use in condensed matter research.

This research has been carried out under the Graduate University beam time proposal PF-02 and PF-26. The author is grateful to Professor R. Colella of Purdue University for stimulating discussions on N-beam dynamical theory of X-ray diffraction.

References

Beaumont, J. H. & Hart, M. (1974). *J. Phys. E*, **7**, 823–824.
Bond, W. L. (1960). *Acta Cryst.* **13**, 814–818.
Cermek, J. (1960). *Acta Cryst.* **13**, 832–835.
Cernohorsky, M. (1960). *Acta Cryst.* **13**, 823–826.
Colella, R. (1974). *Acta Cryst.* A**30**, 413–423.
Deslattes, R. D. & Henins, A. (1973). *Phys. Rev. Lett.* **31**, 972–974.
De Wolf, P. M. (1960). *Acta Cryst.* **13**, 835–837.
Fukumori, T., Imai, K., Hasegawa, T., Akashi, Y. (1997). *J. Phys. Soc. Jpn*, **66**, 1976–1978.

Okada, Y., Sugiyama, H., Zhang, X. W. & Ando, M. (1998). *Photon Factory Activity Report*, Vol. 16, Part B, p. 167. ISSN 1344–6339.
Parrish, W. (1960). *Acta Cryst.* **13**, 838–840.
Rahman, M. O. (2001). PhD thesis, Graduate University for Advanced Studies, Photon Factory, KEK, Tsukuba, Japan.
Rahman, M. O. & Ando, M. (2001). *Proc. SPIE*, **4407**, 141–145.
Rahman, M. O., Okada, Y., Zhang, X. W., Sugiyama, H., Imai, Y., Nakayama, K., Fujomoto, H., Takano, Y., Yoda, Y. & Ando, M. (1999). *KAZUKA Silicon Forum Proc.* **1**, 175–177.
Rahman, M. O., Sugiyama, H., Zhang, X. W. & Ando, M. (1998). *Photon Factory Activity Report*, Vol. 16, Part B, p. 176. ISSN 1344–6339.
Rahman, M. O., Sugiyama, H., Zhang, X. W., Hyodo, K. & Ando, M. (1999). *Proc. JSSRR*, **12**, 210.
Staumanis, M. E. (1960). *Acta Cryst.* **13**, 818–821.
Usuda, K. (1994). PhD thesis, Graduate University for Advanced Studies, Photon Factory, KEK, Tsukuba, Japan.
Weyerer, H. (1960). *Acta Cryst.* **13**, 821–823.
Wilkens, V. M. (1960). *Acta Cryst.* **13**, 826–828.

 Received 17 July 2001 • Accepted 7 November 2001